

# Dynamical nonlinear higher-order non-Hermitian skin effects and topological trap-skin phase

Motohiko Ezawa

*Department of Applied Physics, University of Tokyo, Hongo 7-3-1, 113-8656, Japan*

We study nonreciprocal nonlinear Schrödinger systems. As a prototype we analyze the Hatano-Nelson model together with a typical nonlinear term introduced and its generalization to two dimensions. We employ the quench dynamics, where a pulse is given to one site and its time evolution is analyzed. It is found that the skin state is always formed due to the nonreciprocal hopping and hence that the system is topological. However, the structure of the skin state is essentially modified by the nonlinear interaction because it favors a self-trapping. Four typically different states emerge as an interplay between these two interactions, depending how the pulse is trapped to the initial site. They are the skin, trap-skin, shifted-trap-skin and embedded-trap-skin states, forming four phases in the one-dimensional model. The phase boundary is determined by a gap in terms of certain phase indicators. On the other hand, we find three phases with the shifted-trap-skin phase being absent in the two-dimensional model.

## I. INTRODUCTION

Non-Hermitian topological physics is one of the most exciting fields of current condensed matter physics[1–19]. Among them, the skin state is prominent[12, 19–28], which is absent in the Hermitian systems. All the states are localized at one edge in the skin state for a finite chain. The skin state is generated in a nonreciprocal hopping model, where the amplitudes of the right-going and left-going hoppings are different. It is generalized to higher-order skin states in higher-dimensional systems[19, 27, 29, 30]. On the other hand, nonlinear physics attracts renewed interests in the context of topological physics. It is studied in mechanical[31–33], photonic[34–43], electric circuit[44–46] and resonator[47] systems.

It is interesting and important to explore systems in which nonreciprocity and nonlinearity coexist to reveal phenomena ascribed to their competition and collaboration. Photonic system provides us with a typical playground[34, 35, 48–65], where the nonreciprocal hopping is realized based on coupled resonant optical waveguides[66, 67] and the nonlinearity is introduced by the Kerr effect[68, 69].

In this paper, as a prototype of such systems, we analyze the Hatano-Nelson model[70] modified to include a typical nonlinear term. We also analyzed its generalization to two dimensions. It is an intriguing feature of the models that the topological number of the skin state is given solely by the direction of the localization whether the system is linear or nonlinear. Hence, the skin state is topologically robust how much it is distorted as long as the rightward or leftward localization occurs.

To investigate a rich physics induced by the nonlinear effects, we study the quench dynamics by giving a pulse to one site and exploring the time evolution of the classical field  $\psi_n(t)$  subject to the discrete nonreciprocal nonlinear Schrödinger equation. First, we consider the one-dimensional model. When the nonlinearity is small enough, on the other hand, the initial pulse is pushed toward the right edge, forming a well-known skin state, as in the linear model. When it is strong enough, the pulse is trapped to the initial site together with a formation of the skin state. We call it the trap-skin

state. Novel phenomena occur as an interplay between nonreciprocity and nonlinearity in the intermediate regime. We have found a state where the pulse is trapped not to the initial site but to the adjacent site, which we call the shifted-trap-skin state. We have also found a state where the pulse is trapped to the initial site although it is almost embedded in the skin state. We call it the embedded-trap-skin state. These four different patterns of states occupy some continuous regions in the  $\lambda$ - $\xi$  space with the nonreciprocity strength parameter  $\lambda$  and the nonlinearity strength parameter  $\xi$ . We have thus found four phases, the skin phase, the shifted-trap-skin phase, the embedded-trap-skin phase and the trap-skin phase in the one-dimensional model. The phase indicators are  $S_n$  which are the time average of the amplitude  $|\psi_n(t)|$ , where  $n = m_0$  and  $m_0 + 1$ , with  $m_0$  representing the site to which the pulse is given. The phase boundary is determined by the position of a gap in these phase indicators. On the other hand, we have found that the shifted-trap-skin phase is absent in the two-dimensional model.

## II. ONE-DIMENSIONAL MODEL

### A. Nonlinear skin effect

We propose a one-dimensional discrete nonreciprocal nonlinear Schrödinger equation defined by

$$i \frac{d\psi_n}{dt} + \kappa_R \psi_{n+1} + \kappa_L \psi_{n-1} - (\kappa_R + \kappa_L) \psi_n + \xi |\psi_n|^2 \psi_n = 0, \quad (1)$$

where  $\kappa_R$  and  $\kappa_L$  are the right-going and left-going hopping amplitudes, respectively. It is constructed by introducing a typical nonlinear term to the Hatano-Nelson model[70]. The system is nonreciprocal if  $\kappa_R \neq \kappa_L$ . The nonlinearity is controlled by the parameter  $\xi$ , where large  $\xi$  indicates strong nonlinearity.

We parametrize

$$\kappa_R = \kappa(1 + \lambda), \quad \kappa_L = \kappa(1 - \lambda), \quad (2)$$

where  $\lambda$  is referred to as the nonreciprocity,  $-1 < \lambda < 1$ .

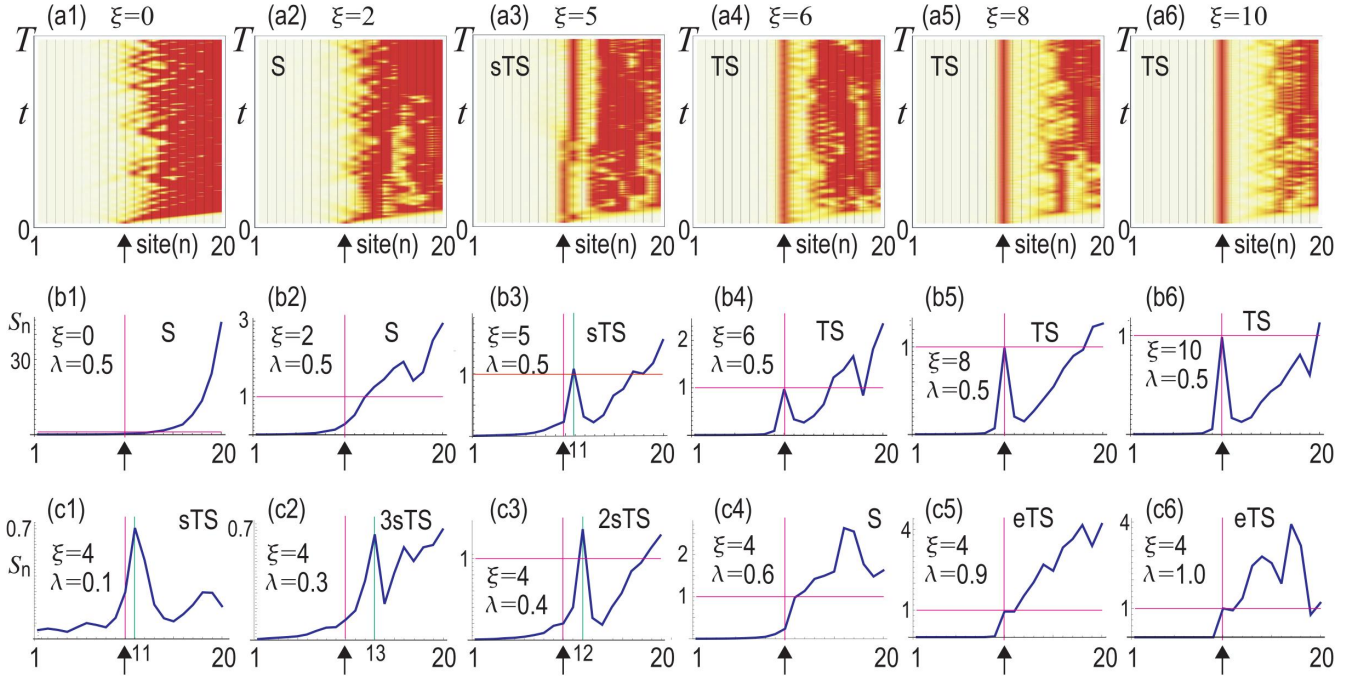


FIG. 1. (a1)~(a6) Time evolution of the amplitude  $|\psi_n(t)|$  from  $t = 0$  to  $t = T$  for various nonlinearity  $\xi$  at fixed nonreciprocity  $\lambda = 0.5$ . The horizontal axis is the site index  $n$ , and the vertical axis is time  $t$ . The color density indicates the magnitude of  $|\psi_n(t)|$ . (b1)~(b6) Time average  $S_n$  of the amplitude defined by Eq.(16) for various  $\xi$  at fixed  $\lambda = 0.5$ . (c1)~(c6) Time average  $S_n$  for various  $\lambda$  at fixed  $\xi = 4$ . The horizontal axis is the site index  $n$ , and the vertical axis is the time average  $S_n$ . The arrow indicates the initial site  $m_0 = L/2 = 10$  from which the quench dynamics starts. We have set  $\kappa = 1$ ,  $L = 20$  and  $T = 50$  in units of  $1/\kappa$ . Symbols S, TS, sTS, eTS stand for the skin, trap-skin, shifted-trap-skin and embedded-trap-skin states, respectively.

## B. Quench dynamics

Quench dynamics provides us with a good signal to detect various phases[71], which is applicable to nonlinear systems[33, 40, 42, 46] as well. Let us study a quench dynamics starting from the site indexed by  $m_0$ ,

$$\psi_n(t) = \delta_{n,m_0} \quad \text{at } t = 0. \quad (3)$$

Here, we take the site  $m_0$  at the center of the sample, i.e.,  $m_0 = L/2$  for a finite chain with size  $L$ , and  $m_0 = (L/2, L/2)$  for a finite square with size  $L \times L$ , where  $L$  is an even integer. Namely, solving the dynamical equation (1) under the initial condition (3), we study the time evolution  $\psi_n(t)$  as a function of the system parameters  $\xi$  and  $\lambda$ .

## C. Linear model

The Hatano-Nelson Hamiltonian is given by[70]

$$H_{nm} = \kappa_R \delta_{n,m+1} + \kappa_L \delta_{n,m-1} - (\kappa_R + \kappa_L) \delta_{n,m}. \quad (4)$$

The eigenenergy is given in the momentum space by

$$E(k) = \kappa_R e^{ik} + \kappa_L e^{-ik} - (\kappa_R + \kappa_L), \quad (5)$$

which is complex for  $\kappa_R \neq \kappa_L$ . The system is analytically solvable.

In the case of a finite chain, the skin state is generated at the left edge and given by

$$\psi_{2n+1} = \left( -\frac{\kappa_R}{\kappa_L} \right)^n \psi_1, \quad \psi_{2n} = 0 \quad (6)$$

for  $|\kappa_L| > |\kappa_R|$ , while it is generated at the right edge and given by

$$\psi_{L-2n} = \left( -\frac{\kappa_L}{\kappa_R} \right)^n \psi_L, \quad \psi_{2n-1} = 0. \quad (7)$$

for  $|\kappa_L| < |\kappa_R|$ .

The dynamical Hatano-Nelson model is defined by

$$i \frac{d\psi_n}{dt} + H_{nm} \psi_m = 0, \quad (8)$$

which is Eq.(1) without the nonlinear term. The quench dynamics of this linear model is exactly solvable in the case of an infinite chain. Indeed, an analytic solution of the quench dynamics based on Eq.(8) is constructed as

$$\psi_n(t) = \left( i \sqrt{\frac{\kappa_L}{\kappa_R}} \right)^{n-m_0} J_{|n-m_0|} (2\sqrt{\kappa_L \kappa_R} t), \quad (9)$$

where  $m_0$  represents the initial site as in Eq.(3) and  $J_{|n-m_0|}$  is the Bessel function of the first kind. It is straightforward

to check that Eq.(9) satisfies the dynamical Hatano-Nelson model (8) together with the initial condition (3) with the aid of the formula

$$\frac{d}{dt}\Psi_n(at) = \frac{ia}{2} \left[ \gamma\Psi_{n-1}(at) + \frac{1}{\gamma}\Psi_{n+1}(at) \right], \quad (10)$$

where  $\Psi_n(t) \equiv (i\gamma)^n J_n(at)$  with an arbitrary constant  $a$ .

#### D. Topological number

The Hatano-Nelson model has only one band as in Eq.(5) and there is no "gap" in the usual acceptance of the Hermitian model. Nevertheless, it is possible to define the topological number with the aid of the complex degrees of freedom present in the energy[11]. Indeed, the structure of the band (5) is an ellipse in the complex plane as illustrated in Fig.2. Such a band is said to have a point gap[12, 72]. The following observation is essential. As the momentum runs from  $k = 0$  to  $2\pi$ , the band energy  $E(k)$  encircles the ellipse once. Furthermore, the direction of the winding is opposite for  $\lambda > 0$  and  $\lambda < 0$ , or  $|\kappa_L| < |\kappa_R|$  and  $|\kappa_L| > |\kappa_R|$ . This property allows us to define the topological number.

The topological number is defined in the Hatano-Nelson model by the winding number in the complex-energy plane as[11, 12]

$$w = \int_0^{2\pi} \frac{dk}{2\pi} \partial_k \ln [E(\mathbf{k}) - \bar{E}], \quad (11)$$

where  $\bar{E}$  is the mean energy,

$$\bar{E} = \int_0^{2\pi} \frac{dk}{2\pi} E(\mathbf{k}) = -(\kappa_R + \kappa_L). \quad (12)$$

It yields  $w = 1$  for  $|\kappa_L| < |\kappa_R|$  and  $w = -1$  for  $|\kappa_L| > |\kappa_R|$ . Furthermore, we have  $w = 0$  for  $\kappa_L = \kappa_R$ , because  $E(\mathbf{k})$  is single-valued. It is understood as the vorticity of the energy[11].

The topological number is rewritten as

$$w = \text{sgn}(|\psi_L| - |\psi_1|), \quad (13)$$

in terms of the amplitudes at the left and right edges of a finite chain. This formula is valid even for nonlinear systems. The system is topological for  $\kappa_L \neq \kappa_R$  and trivial for  $\kappa_L = \kappa_R$ .

It is an intriguing feature of the Hatano-Nelson type models that the topological number is determined solely by the direction of the localization in the skin state based on the formula (13). Namely, the skin state is topologically robust how much it is distorted as long as the rightward or leftward localization occurs. We will numerically check the robustness against disorders in Subsection II H.

#### E. Strong nonlinear model

We next study the strong nonlinear model, where we neglect the hopping term with respect to the nonlinear term. We

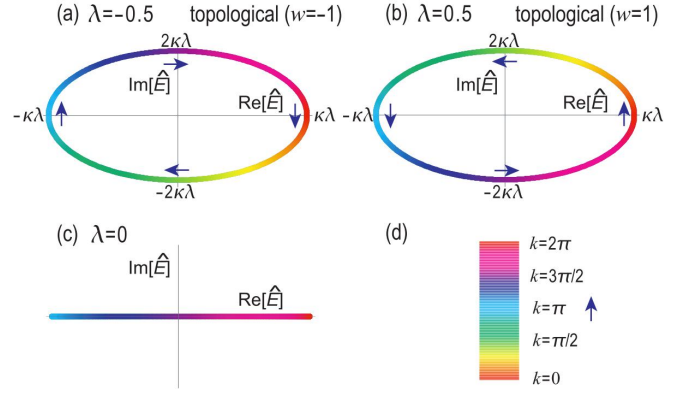


FIG. 2. Band structure in the  $\text{Re}[\hat{E}]-\text{Im}[\hat{E}]$  plane, where  $\hat{E} \equiv E(\mathbf{k}) - \bar{E}$  at (a)  $\lambda = -0.5$  with  $w = -1$ , (b)  $\lambda = 0.5$  with  $w = 1$ , and (c)  $\lambda = 0$  with  $w = 0$ . Here,  $w$  is the winding number. (d) The color palette indicates the momentum  $k$  for (a), (b) and (c). The arrow indicates the direction for  $k$  to increase.

approximate Eq.(1) as

$$i \frac{d\psi_n}{dt} = -\xi |\psi_n|^2 \psi_n, \quad (14)$$

where all equations are separated one another. This system is also analytically solvable.

We set  $\psi_n(t) = r_n e^{i\theta_n(t)}$ , and make an ansatz that  $r_n$  is a constant in the time  $t$ . Then, the solution is given by  $\theta_n = \xi r_n^2 t + c$ . Due to the initial conservation (3), we find

$$|\psi_n(t)| = \delta_{nm_0}. \quad (15)$$

Hence, the initial pulse is trapped to the initial site  $n = m$ . This phase may be referred to as the trap phase.

#### F. Four different skin states

We show the amplitude  $|\psi_n|$  in Fig.1 for various  $\xi$  at fixed  $\lambda = 0.5$ , and also for various  $\lambda > 0$  at fixed  $\xi = 4$ , by numerically solving the quench dynamics subject to the equation of motion (1) with the initial condition (3). The time evolution is given in Figs.1(a1)~(a6) for each site  $n$ , where the value of  $|\psi_n|$  is indicated by the darkness of color.

There is a characteristic behavior at the initial stage for each set of  $\xi$  and  $\lambda$ . To remove it and to reveal a more quantitative structure of the amplitude, we define the time average of its site dependence over a time span from  $T/2$  to  $T$  by

$$S_n \equiv \frac{1}{T/2} \int_{T/2}^T |\psi_n(t)| dt, \quad (16)$$

and show it in Figs.1(b1)~(b6) and (c1)~(c6) for each site  $n$ .

As a general structure, the wave packet shifts rightward (leftward) when the right-going hopping is larger (smaller) than the left-going hopping, forming a skin state irrespective of  $\lambda$  and  $\xi$ . Hence, the system is always in the skin phase and topological with  $w = 1$  for  $\lambda > 0$  or  $|\kappa_R| > |\kappa_L|$ , and with

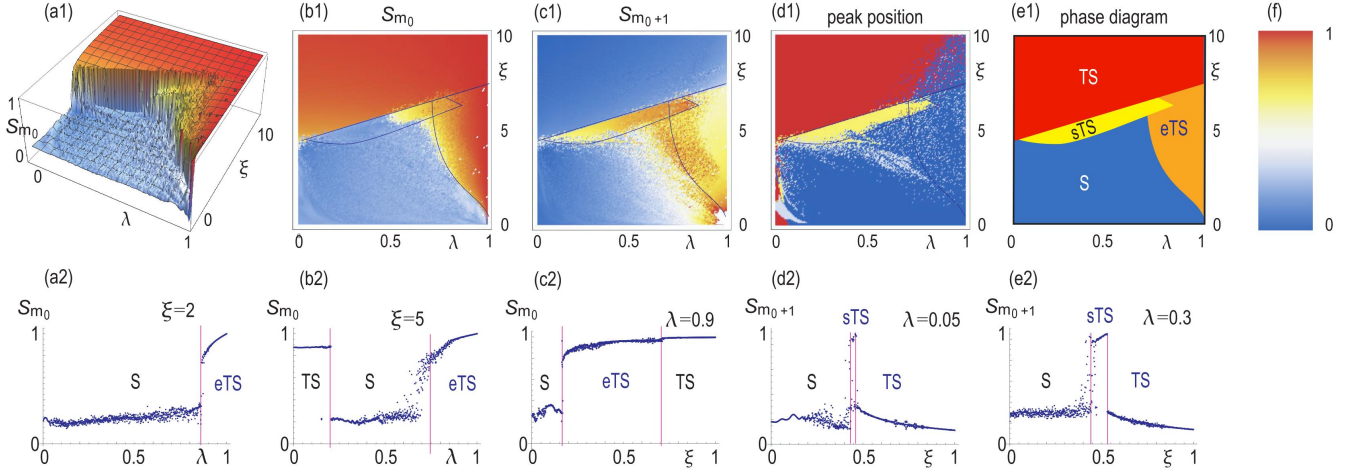


FIG. 3. (a1) and (b1) Time average  $S_{m_0}$  of the amplitude as a function of the nonreciprocity  $\lambda$  and the nonlinearity  $\xi$  in the one-dimensional model, with (a1) being a bird's eye's view. The red region represents  $S_{m_0} = 1$ , while the blue region represents  $S_{m_0} = 0$ . (c1) The time average  $S_{m_0+1}$  differentiates the trap-skin (TS) phase from all others. The embedded-trap-skin (eTS) phase is assigned from (b1) and (c1). (d1) Positions of the maximum among  $S_{m_0}, S_{m_0+1}, S_{m_0+2}$  and  $S_{m_0+3}$  are shown, where the maximum is taken at  $S_{m_0}$  in the red region, at  $S_{m_0+1}$  in the yellow region, at  $S_{m_0+2}$  in the white region, and at  $S_{m_0+3}$  in the blue region. The shifted-trap-skin (sTS) phase is assigned from (c1) and (d1). (e1) Phase diagram in the  $\lambda$ - $\xi$  plane. (a2)~(e2) Typical examples of the average  $S_{m_0}$  or  $S_{m_0+1}$  as a function of  $\lambda$  at a fixed value of  $\xi$  or a function of  $\xi$  at a fixed value of  $\lambda$ . The phase boundary is determined by the position of a gap. We have set  $\kappa = 1$  and  $L = 20$ . (f) The color palette indicates the amplitude in (a1), (b1) and (c1).

$w = -1$  for  $\lambda < 0$  or  $|\kappa_R| < |\kappa_L|$  even in the nonlinear system according to the formula (13). We assume  $\lambda > 0$  in what follows.

There are typically four different patterns in the skin states generated by the nonlinearity effects as described below:

(1) The standard skin states emerge as in Figs.1(b1)~(b2) and (c4). We call it the skin (S) state.

(2) In addition to the formation of the skin state, the initial pulse is trapped to the initial site as in Figs.1(b4)~(b6). Namely, it is a coexistent system of the skin state and the trap state. The characteristic feature is that the equality  $S_{m_0} = 1$  keeps to hold as a reminiscence of the initial condition (3). We call it the trap-skin (TS) state.

(3) In addition to the formation of the trap-skin state, the initial pulse is trapped not to the initial site but to a site near to it as in Figs.1(b3) and (c1)~(c3). Let us call it the  $n$ -site-shifted-trap-skin state, and abbreviate it as the  $ns$ TS state, when the trap site is away from the original site by  $n$  sites. When  $n = 1$ , we call it simply the sTS state.

(4) The skin state develops over a wide region including the initial state  $m_0$  as in Figs.1(c5)~(c6). Although it looks just as if it were the standard skin state, the equality  $S_{m_0} = 1$  keeps to hold as a reminiscence of the initial condition (3). We call it the embedded-trap-skin (eTS) state.

### G. Phase diagram

We have pointed out the emergence of four types of the skin states depending on  $\lambda$  and  $\xi$ . Let us construct a phase diagram in the  $\lambda$ - $\xi$  space. First, we focus on the time average  $S_{m_0}$ , and show it as a function of  $\lambda$  and  $\xi$  in Figs.3(a1) and (b1), where

Fig.3(a1) is a bird's eye's view.

Fig.3(b1) may present a rough picture of the phase diagram, where the blue region is the skin phase while the red region is the trap phase. However, it is impossible to differentiate the trap-skin and the embedded-trap-skin states in Fig.3(b1) because  $S_{m_0} = 1$  for both states. Furthermore, the transition between the skin and trap phases is blurred around  $\lambda = 0.6$  and  $\xi = 0.6$ .

They are differentiated by the indicator  $S_{m_0+1}$ , whose results are shown in Fig.3(c1). Note that  $S_{m_0+1}$  is almost zero for the trap-skin state but takes a larger value for the shifted-trap-skin state. The phase boundary is linear as a function of  $\lambda$  in Fig.3(c1). It is understood as follows. The hopping motion is enhanced as a function of the nonreciprocity  $\lambda$  as in Eq.(2). On the other hand, it is depressed as a function of the nonlinearity  $\xi$  because it favors the trap state.

Next, we plot the position of the peak among  $S_{m_0}, S_{m_0+1}, S_{m_0+2}$  and  $S_{m_0+3}$ . If the peak position is at  $S_{m_0}$ , it is the trap-skin state depicted in red. If it is at  $S_{m_0+n}$ , it is the  $n$ -site-shifted-trap-skin state depicted in yellow for  $n = 1$ , in white for  $n = 2$ , in blue for  $n = 3$ . We find one-site-shifted-trap-skin states form a region in the vicinity of the trap-skin state. On the other hand,  $n$ -site-shifted-trap-skin states do not form a continuous region for  $n = 2$  and 3. Note that 3-site-shifted-trap-skin states are buried in the skin phase and hardly identified.

We thus obtain a phase diagram as in Fig.3(e1). In determining phase boundaries, we have calculated  $S_{m_0}$  and  $S_{m_0+1}$  as a function of  $\lambda$  for a fixed value of  $\xi$  as in Figs.3(a2) and (b2), and also as a function of  $\xi$  for a fixed value of  $\lambda$  as in Figs.3(c2), (d3) and (e2) for many fixed values. Phase transition points are clearly observed as gaps in these figures.



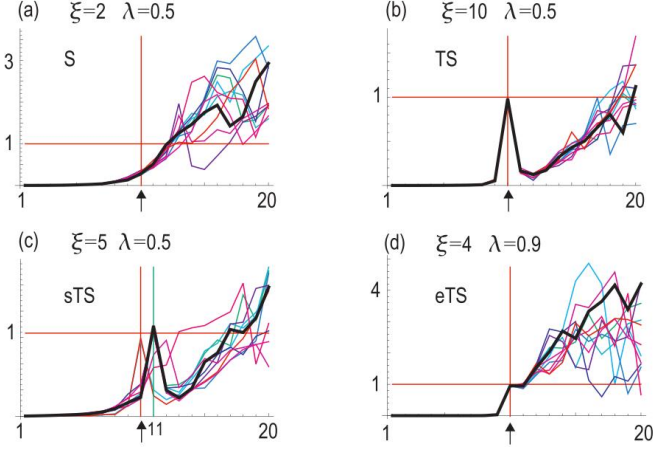


FIG. 4. On-site disorder effects of the time average  $S_n$  for a typical state taken from Fig.3 in each phase: (a)  $\xi = 2, \lambda = 0.5$ , (b)  $\xi = 10, \lambda = 0.5$ , (c)  $\xi = 5, \lambda = 0.5$ , (d)  $\xi = 4, \lambda = 0.9$ . Thick black curves are the amplitudes without disorders. Colored curves are the amplitudes with disorders ranging from  $\zeta = 0.1$  (red) to  $\zeta = 1$  (cyan). We have set  $\kappa = 1$  and  $L = 20$ . See also the caption of Fig.3.

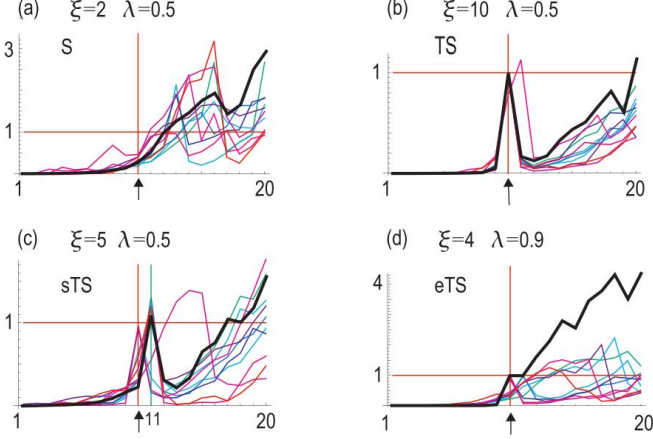


FIG. 5. Hopping disorder effects of the time average  $S_n$  for a typical state taken from Fig.3 in each phase: (a)  $\xi = 2, \lambda = 0.5$ , (b)  $\xi = 10, \lambda = 0.5$ , (c)  $\xi = 5, \lambda = 0.5$ , (d)  $\xi = 4, \lambda = 0.9$ . Thick black curves are the amplitudes without disorders. Colored curves are the amplitudes with disorders ranging from  $\zeta = 0.1$  (red) to  $\zeta = 0.8$  (cyan). We have set  $\kappa = 1$  and  $L = 20$ . See also the caption of Fig.3.

### H. Disorder effects

As we have noted in Subsection IID, the robustness of the topological states and that of the skin states are equivalent in the Hatano-Nelson model. The topological states are well known to be robust against disorders in the linear model. We study and confirm the robustness of topological states in the nonlinear model for three types of disorders, although the phase diagram in Fig.3 is not because the phase indicators are

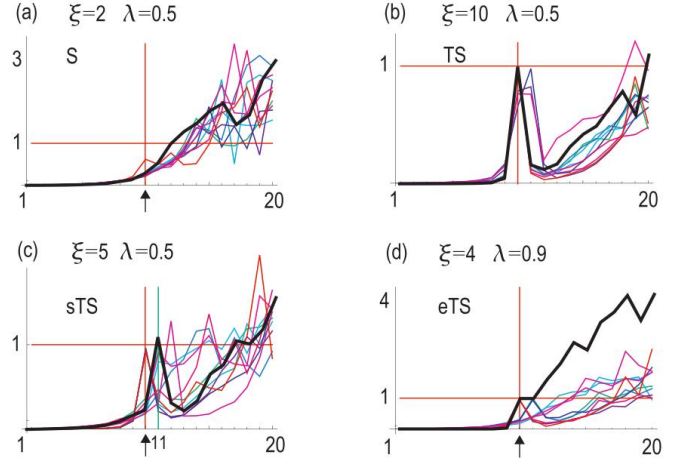


FIG. 6. Nonlinearity disorder effects of the time average  $S_n$  for a typical state taken from Fig.3 in each phase: (a)  $\xi = 2, \lambda = 0.5$ , (b)  $\xi = 10, \lambda = 0.5$ , (c)  $\xi = 5, \lambda = 0.5$ , (d)  $\xi = 4, \lambda = 0.9$ . Thick black curves are the amplitudes without disorders. Colored curves are the amplitudes with disorders ranging from  $\zeta = 0.1$  (red) to  $\zeta = 1$  (cyan). We have set  $\kappa = 1$  and  $L = 20$ . See also the caption of Fig.3.

not topological invariants.

First, we introduce randomness into the on-site potential as

$$V_n = V(1 + \eta_n \zeta), \quad (17)$$

with  $\eta_n$  being a random variable ranging from  $-1$  to  $1$ , and  $\zeta$  is the strength of the disorder. The Hamiltonian is modified as

$$H_{nm} = \kappa_R \delta_{n,m+1} + \kappa_L \delta_{n,m-1} - (\kappa_R + \kappa_L + V_n) \delta_{n,m}, \quad (18)$$

which we analyze numerically. We show the profile of  $S_n$  in Fig.4. We observe some features. Although  $S_n$  is affected significantly near the edge, the overall skin structure is maintained and all states remain to be skin states. Namely, the skin states are robust against disorders even in the nonlinear regime.

Second, we introduce disorders in the hopping

$$H_{nm} = \kappa_{R,n} \delta_{n,m+1} + \kappa_{L,n} \delta_{n,m-1} - (\kappa_{R,n} + \kappa_{L,n} + V_n) \delta_{n,m}, \quad (19)$$

where we have defined

$$\kappa_{R,n} \equiv \kappa_R (1 + \eta_n^R \zeta), \quad \kappa_{L,n} \equiv \kappa_L (1 + \eta_n^L \zeta), \quad (20)$$

with  $\eta_n^R$  and  $\eta_n^L$  being a random variable ranging from  $-1$  to  $1$ . The results are shown in Fig.5. The skin state is largely deformed comparing to the case of the on-site potential. It is natural because the magnitude of the hopping is essential for the skin state. However, the overall skin states are preserved even in the presence of the hopping disorder.

Finally, we introduce disorders in the nonlinearity,

$$i \frac{d\psi_n}{dt} + \kappa_R \psi_{n+1} + \kappa_L \psi_{n-1} - (\kappa_R + \kappa_L) \psi_n + \xi_n |\psi_n|^2 \psi_n = 0, \quad (21)$$

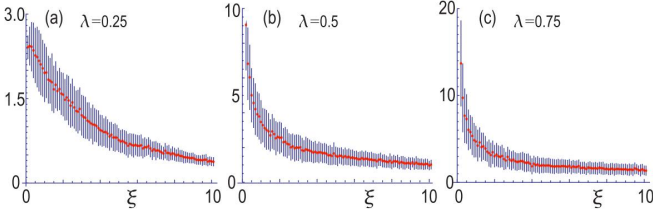


FIG. 7. Dependence of the edge amplitude  $|\psi_L|$  on the nonlinearity  $\xi$  for (a)  $\lambda = 0.25$ , (b)  $\lambda = 0.5$ , and (c)  $\lambda = 0.75$ . It decreases as  $\xi$  increases. We have taken 100 times average on the random on-site potential. The red dots indicate the mean value, while the blue bars indicate the standard deviation. We have set  $\kappa = 1$  and  $L = 20$ .

where we have defined

$$\xi_n \equiv \xi (1 + \eta_n \zeta). \quad (22)$$

The results are shown in Fig.6. We find that the skin state is robust against the nonlinearity disorder.

A comment is in order. The topological number only assures the robustness of the skin state, and not the robustness of the detailed structure of the skin state such as the trap-skin, shifted-trap-skin and embedded-trap-skin states. Actually, they are transformed among them by disorder effects as shown in Figs.4, 5 and 6. This is because the phase indicators are not topological invariants.

### I. Nonlinearity dependence of skin effect

The strength of the skin effect is suppressed as the nonlinearity increases, as shown in Fig.1. The amplitude  $|\psi_L|$  at the right edge is a good signal to estimate it. Its  $\xi$  dependence is shown in Fig.7, where  $|\psi_L|$  decreases as the increase of  $\xi$ . It validates that the skin state is suppressed by the nonlinear effect. It is due to the fact that the nonlinear term prefers the stop of the motion, which makes hard for the initial pulse to hop and form a skin state.

## III. TWO-DIMENSIONAL MODEL

### A. Nonlinear second-order skin effect

A two-dimensional generalization of the nonreciprocal discrete nonlinear Schrödinger equation (1) reads

$$i \frac{d\psi_n}{dt} + \kappa_R \psi_{n+x} + \kappa_L \psi_{n-x} + \kappa_U \psi_{n+y} + \kappa_D \psi_{n-y} = (\kappa_R + \kappa_L + \kappa_U + \kappa_D) \psi_n - \xi |\psi_n|^2 \psi_n, \quad (23)$$

by introducing the upward and downward hopping amplitudes  $\kappa_U$  and  $\kappa_D$ , respectively, in addition to  $\kappa_R$  and  $\kappa_L$ . We show the time evolution of the spatial distribution of the amplitude  $|\psi_n|$  in Fig.8.

### B. Linear model

We study the linear model with  $\xi = 0$ . In the momentum space, the energy is given by

$$E(k_x, k_y) = \kappa_R e^{ik_x} + \kappa_L e^{-ik_x} + \kappa_U e^{ik_y} + \kappa_D e^{-ik_y} - (\kappa_R + \kappa_L + \kappa_U + \kappa_D). \quad (24)$$

When  $|\kappa_R| < |\kappa_L|$  and  $|\kappa_U| < |\kappa_D|$  in the case of a finite square, a corner-skin state is generated at the left-down corner, whose eigenfunction of the linear model is given by

$$\psi_{2n_x+1, 2n_y+1} = \left(-\frac{\kappa_R}{\kappa_L}\right)^{n_x} \left(-\frac{\kappa_U}{\kappa_D}\right)^{n_y} \psi_{1,1}, \quad (25)$$

and otherwise  $\psi_{n,m} = 0$ . All other corner-skin states are obtained in a similar manner.

### C. Topological number

The topological number is defined in the linear model by

$$w_\mu = \int_{-\pi}^{\pi} \frac{dk_\mu}{2\pi i} \partial_{k_\mu} \ln [E(k_x, k_y) - \bar{E}_\mu], \quad (26)$$

where

$$\bar{E}_\mu = \int_{-\pi}^{\pi} \frac{dk_\mu}{2\pi} E(k_x, k_y) \quad (27)$$

with  $\mu = x, y$ . We note that  $E(k_x, k_y) - \bar{E}_\mu$  only depends on  $k_\mu$ . They are explicitly given by

$$E(k_x, k_y) - \bar{E}_x = \kappa_R e^{ik_x} + \kappa_L e^{-ik_x}, \quad (28)$$

$$E(k_x, k_y) - \bar{E}_y = \kappa_U e^{ik_y} + \kappa_D e^{-ik_y}. \quad (29)$$

The topological numbers are also rewritten as

$$w_x = \text{sgn}(|\psi_{L,L}| + |\psi_{L,1}| - |\psi_{1,L}| - |\psi_{1,1}|), \quad (30)$$

$$w_y = \text{sgn}(|\psi_{L,L}| - |\psi_{L,1}| + |\psi_{1,L}| - |\psi_{1,1}|), \quad (31)$$

in a finite square system. If  $\kappa_R = \kappa_U$  and  $\kappa_L = \kappa_D$ , they are simply given by

$$w_x = w_y = \text{sgn}(|\psi_{L,L}| - |\psi_{1,1}|), \quad (32)$$

because we have  $|\psi_{L,1}| = |\psi_{1,L}|$ . It means that there are only two phases, where the skin states emerge at the right-up corner or the left-down corner.

We have  $w_x = 1$  for  $|\kappa_L| < |\kappa_R|$  and  $w_x = -1$  for  $|\kappa_L| > |\kappa_R|$ , while we have  $w_y = 1$  for  $|\kappa_D| < |\kappa_U|$  and  $w_y = -1$  for  $|\kappa_D| > |\kappa_U|$ . There are four topological phases  $(w_x, w_y) = (\pm 1, \pm 1)$ . The corner skin state emerges at the right-up corner for  $(w_x, w_y) = (1, 1)$ , at the right-down corner for  $(w_x, w_y) = (1, -1)$ , at the left-up corner for  $(w_x, w_y) = (-1, 1)$  and at the left-down corner for  $(w_x, w_y) = (-1, -1)$ . These formulas are valid also in the nonlinear models. The system is always topological unless  $\kappa_L = \kappa_R$  and  $\kappa_D = \kappa_U$ .

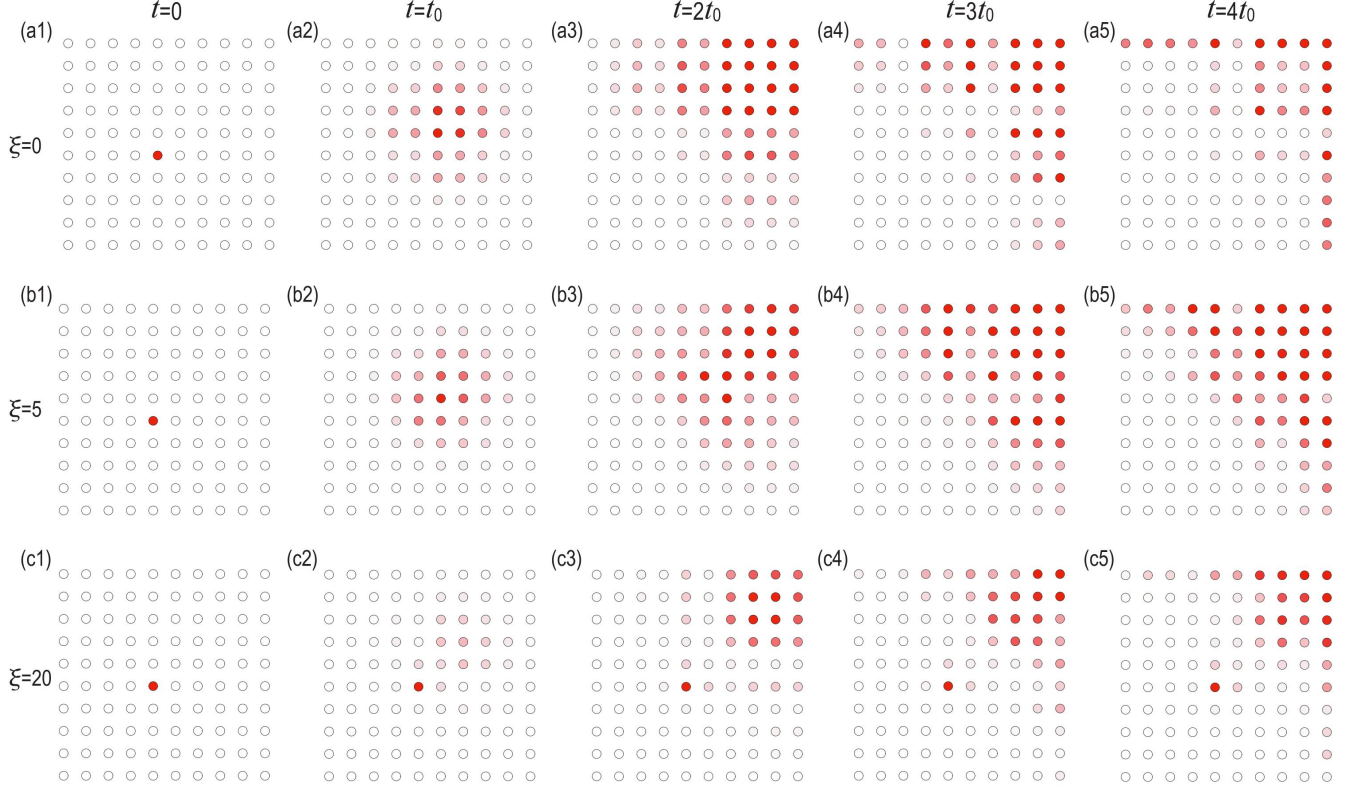


FIG. 8. Time evolution of the spatial distribution of the amplitude  $|\psi_n|$  in the two-dimensional model for (a1)~(a5)  $\xi = 0$ , (b1)~(b5)  $\xi = 5$ , and (c1)~(c5)  $\xi = 20$ , when the quench dynamics starts from the site indicated in red at  $t = 0$ . The color density indicates the amplitude  $|\psi_n|$ . We have set  $\kappa_R = \kappa_U = 1.5$  and  $\kappa_L = \kappa_D = 0.5$ . We have set  $\lambda = 0.5$ ,  $L = 10$ . The time step is  $t_0 = 1$  and the simulation time is  $T = 10$  in units of  $1/\kappa$ .

#### D. Quench dynamics

We find an analytic solution of the quench dynamics for the linear model (23) with  $\xi = 0$  as

$$\psi_{n_x, n_y}(t) = \left( i \sqrt{\frac{\kappa_L}{\kappa_R}} \right)^{n_x} \left( i \sqrt{\frac{\kappa_D}{\kappa_U}} \right)^{n_y} \times J_{|n_x|} (2\sqrt{\kappa_L \kappa_R} t) J_{|n_y|} (2\sqrt{\kappa_D \kappa_U} t), \quad (33)$$

where it starts from a localized site  $m_0 = (0, 0)$  in an infinite square lattice.

The quench dynamics is numerically studied for the non-linear model (23), where it starts from a localized site  $m_0 = (L/2, L/2)$  in a finite square lattice. We show the results in Fig.8. At the initial stage, the peak of the amplitude shifts to the up-right direction. Once it reaches the right-up corner, the state almost remains as it is although there are fluctuations due to the reflection at the edges. It is a generalization of the result of the one-dimensional case discussed before.

#### E. Phase diagram

We define the time average  $S_{m_0, m_0}$  by a straightforward generalization of Eq.(16). We show it as a function of the nonreciprocity  $\lambda$  and the nonlinearity  $\xi$  in Figs.9(a) and (b),

where Fig.9(a) is a bird's eye's view. The blue region indicates the skin phase. We also plot  $\Delta S \equiv S_{m_0, m_0} - S_{m_0, m_0+1}$  in Fig.9(c), which differentiates the trap-skin and the embedded-trap-skin states. As in the case of the one-dimensional model, there are skin, trap-skin and embedded-trap-skin states in the phase diagram. On the other hand, there is no shifted-trap-skin state in the two-dimensional model. It may be due to the fact that there is a large degree of freedom to hop in the two-dimensional model in contrast to the one-dimensional model, which makes harder for the initial pulse to form a shifted-trap-skin state but results in just an ordinary skin state. We thus obtain a phase diagram as in Fig.9(d).

### IV. DISCUSSIONS

We have studied models in which nonreciprocity and non-linearity coexist. Skin states emerge irrespective of the nonlinearity, which implies that the system is always topological. Additionally, we have found four typically different states generated by the nonlinearity effect in the one-dimensional model. They are the trap-skin, shifted-trap-skin and embedded-trap-skin states, forming four phases.

Two comments are in order. First, skin states are also formed at dislocations[73, 74]. It is an interesting problem to

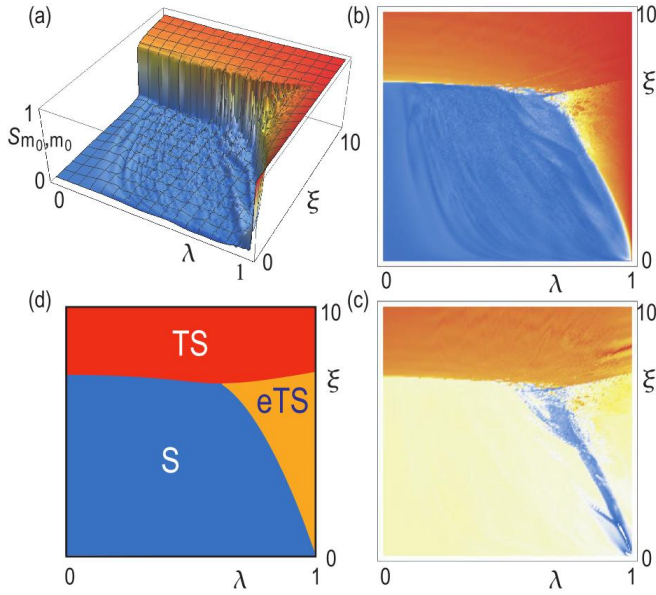


FIG. 9. (a) and (b) Time average  $S_{m_0, m_0}$  of the amplitude as a function of the nonreciprocity  $\lambda$  and the nonlinearity  $\xi$  in the two-dimensional model, with (a) being a bird's eye's view. The red region indicates the trap-skin (TS) phase or the embedded-trap-skin (eTS) phase where  $S_{m_0, m_0} = 1$ , while the blue region represents the skin phase where  $S_{m_0, m_0} = 0$ . (c) The time average of the difference  $\Delta S = S_{m_0, m_0} - S_{m_0, m_0+1}$ , which differentiates the eTS phase from the TS phase. (d) Phase diagram in the  $\lambda$ - $\xi$  plane. We have set  $L = 10$  and  $T = 10$ . The color palette of (a), (b) and (c) is the same as Fig.3(f).

study nonlinear skin effect in systems with dislocations. Second, nonlinear non-Hermitian skin states are studied recently in the frequency space[75]. However, the four phases above mentioned are not found in this work. In addition, there is no generalization to nonlinear higher-order skin states. The quench method reveals a rich phase diagram of the nonlinear nonreciprocal system.

The author is very much grateful to S. Iwamoto and N. Nagaosa for helpful discussions on the subject. This work is supported by the Grants-in-Aid for Scientific Research from MEXT KAKENHI (Grants No. JP17K05490 and No. JP18H03676). This work is also supported by CREST, JST (JPMJCR16F1 and JPMJCR20T2).

- 
- [1] C. M. Bender and S. Boettcher, Phys. Rev. Lett. 80, 5243 (1998).
  - [2] C. M. Bender, D. C. Brody, and H. F. Jones, Phys. Rev. Lett. 89, 270401 (2002).
  - [3] K. Esaki, M. Sato, K. Hasebe, and M. Kohmoto, Phys. Rev. B 84, 205128 (2011).
  - [4] H. Schomerus, Opt. Lett. 38, 1912 (2013).
  - [5] S. Weimann, M. Kremer, Y. Plotnik, Y. Lumer, S. Nolte, K. G. Makris, M. Segev, M. C. Rechtsman, and A. Szameit, Nat. Mater. 16, 433 (2017).
  - [6] S.-D. Liang and G.-Y. Huang, Phys. Rev. A 87, 012118 (2013).
  - [7] M. Pan, H. Zhao, P. Miao, S. Longhi, and L. Feng, Nat. Commun. 9, 1308 (2018).
  - [8] D. Leykam, K. Y. Bliokh, Chunli Huang, Y. D. Chong, and Franco Nori, Phys. Rev. Lett. 118, 040401 (2017).
  - [9] B. Zhu, R. Lu and S. Chen, Phys. Rev. A 89, 062102 (2014).
  - [10] V. V. Konotop, J. Yang, and D. A. Zezyulin, Rev. Mod. Phys. 88, 035002 (2016).
  - [11] H. Shen, B. Zhen and L. Fu, Phys. Rev. Lett. 120, 146402 (2018)
  - [12] Z. Gong, Y. Ashida, K. Kawabata, K. Takasan, S. Higashikawa and M. Ueda, Phys. Rev. X 8, 031079 (2018).
  - [13] R. El-Ganainy, K. G. Makris, M. Khajavikhan, Z. H. Musslimani, S. Rotter and D. N. Christodoulides, Nat. Physics 14, 11 (2018).
  - [14] K. Kawabata, Y. Ashida, H. Katsura, M. Ueda, Phys. Rev. B 98, 085116 (2018).
  - [15] C. Yuce, Phys. Rev. A 97, 042118 (2018).
  - [16] L.-J. Lang, Y. Wang, H. Wang, Y. D. Chong, Phys. Rev. B 98, 094307 (2018).
  - [17] T. Liu, Y.-R. Zhang, Q. Ai, Z. Gong, K. Kawabata, M. Ueda, F. Nori, Phys. Rev. Lett. 122, 076801 (2019).
  - [18] M. Ezawa, Phys. Rev. B 99, 201411(R) (2019).
  - [19] M. Ezawa, Phys. Rev. B 99, 121411(R) (2019).
  - [20] Y. Xiong, J. Physics Communications 2, 035043 (2018).
  - [21] V. M. Martinez Alvarez, J. E. Barrios Vargas, and L. E. F. Foa Torres, Phys. Rev. B 97, 121401 (2018).
  - [22] F. K. Kunst, E. Edvardsson, J. C. Budich and E. J. Bergholtz, Phys. Rev. Lett. 121, 026808 (2018).
  - [23] S. Yao and Z. Wang, Phys. Rev. Lett. 121, 086803 (2018).
  - [24] C. H. Lee, R. Thomale, Phys. Rev. B 99, 201103 (2019).
  - [25] L. Jin and Z. Song, Phys. Rev. B 99, 081103 (2019).
  - [26] K. Luo, R. Yu, and H. Weng, Research 2018, ID 6793752
  - [27] C. H. Lee, L. Li and J. Gong, Phys. Rev. Lett. 123, 016805 (2019).
  - [28] K. Luo, J. Feng, Y. X. Zhao, and R. Yu, Phys. Rev. Lett. 123, 016805 (2019).
  - [29] K. Kawabata, M. Sato, and K. Shiozaki, Phys. Rev. B 102, 205118 (2020).
  - [30] R. Okugawa, R. Takahashi and K. Yokomizo, Phys. Rev. B 102, 241202(R) (2020).
  - [31] D. D. J. M. Sneek, Y.-P. Ma, Extreme Mechanics Letters 100487 (2019).
  - [32] P.-W. Lo, K. Roychowdhury, B. G.-g. Chen, C. D. Santangelo,



- C.-M. Jian, M. J. Lawler, Phys. Rev. Lett. **127**, 076802 (2021).
- [33] M. Ezawa, J. Phys. Soc. Jpn. **90**, 114605 (2021).
- [34] D. Leykam and Y. D. Chong, Phys. Rev. Lett. **117**, 143901 (2016).
- [35] X. Zhou, Y. Wang, D. Leykam and Y. D. Chong, New J. Phys. **19**, 095002 (2017).
- [36] L. J. Maczewsky, M. Heinrich, M. Kremer, S. K. Ivanov, M. Ehrhardt, F. Martinez, Y. V. Kartashov, V. V. Konotop, L. Torner, D. Bauer, A. Szameit, Science **370**, 701 (2010).
- [37] D. Smirnova, D. Leykam, Y. Chong and Y. Kivshar, Applied Physics Reviews **7**, 021306 (2020).
- [38] T. Tuloup, R. W. Bomantara, C. H. Lee and J. Gong, Phys. Rev. B **102**, 115411 (2020).
- [39] S. Kruk, A. Poddubny, D. Smirnova, L. Wang, A. Slobozhanyuk, A. Shorokhov, I. Kravchenko, B. Luther-Davies and Y. Kivshar, Nature Nanotechnology **14**, 126 (2019).
- [40] M. Ezawa, Phys. Rev. B **104**, 235420 (2021).
- [41] M. S. Kirsch, Y. Zhang, M. Kremer, L. J. Maczewsky, S. K. Ivanov, Y. V. Kartashov, L. Torner, D. Bauer, A. Szameit and M. Heinrich, Nature Physics **17**, 995 (2021).
- [42] M. Ezawa, cond-mat/arXiv:2110.15602
- [43] M. Ezawa, Phys. Rev. Research **4**, 013195 (2022)
- [44] Y. Hadad, J. C. Soric, A. B. Khanikaev, and A. Alù, Nature Electronics **1**, 178 (2018).
- [45] K. Sone, Y. Ashida, T. Sagawa, arXiv:2012.09479
- [46] M. Ezawa, J. Phys. Soc. Jpn. **91**, 024703 (2022)
- [47] F. Zangeneh-Nejad and R. Fleury, Phys. Rev. Lett. **123**, 053902 (2019).
- [48] A. B. Khanikaev, S. H. Mousavi, W.-K. Tse, M. Kargarian, A. H. MacDonald, G. Shvets, Nature Materials **12**, 233 (2013).
- [49] M. Hafezi, E. Demler, M. Lukin, J. Taylor, Nature Physics **7**, 907 (2011).
- [50] M. Hafezi, S. Mittal, J. Fan, A. Migdall, J. Taylor, Nature Photonics **7**, 1001 (2013).
- [51] L.H. Wu and X. Hu, Phys. Rev. Lett. **114**, 223901 (2015).
- [52] L. Lu, J. D. Joannopoulos and M. Soljacic, Nature Photonics **8**, 821 (2014).
- [53] T. Ozawa, H. M. Price, N. Goldman, O. Zilberberg and I. Carusotto Phys. Rev. A **93**, 043827 (2016).
- [54] A. B. Khanikaev and G. Shvets, Nature Photonics **11**, 763 (2017).
- [55] P. St-Jean, V. Goblot, E. Galopin, A. Lemaitre, T. Ozawa, L. Le Gratiet, I. Sagnes, J. Bloch and A. Amo, Nature Photonics **11**, 651 (2017).
- [56] Y. Ota, R. Katsumi, K. Watanabe, S. Iwamoto and Y. Arakawa, Communications Physics **1**, 86 (2018)
- [57] T. Ozawa, H. M. Price, A. Amo, N. Goldman, M. Hafezi, L. Lu, M. C. Rechtsman, D. Schuster, J. Simon, O. Zilberberg and L. Carusotto, Rev. Mod. Phys. **91**, 015006 (2019).
- [58] Y. Ota, F. Liu, R. Katsumi, K. Watanabe, K. Wakabayashi, Y. Arakawa and S. Iwamoto, Optica **6**, 786 (2019).
- [59] T. Ozawa and H. M. Price, Nature Reviews Physics **1**, 349 (2019).
- [60] A. E. Hassan, F. K. Kunst, A. Moritz, G. Andler, E. J. Bergholtz, M. Bourennane, Nature Photonics **13**, 697 (2019).
- [61] Y. Ota, K. Takata, T. Ozawa, A. Amo, Z. Jia, B. Kante, M. Notomi, Y. Arakawa, S. Iwamoto, Nanophotonics **9**, 547 (2020).
- [62] M. Li, D. Zhirihin, D. Filonov, X. Ni, A. Slobozhanyuk, A. Alu and A. B. Khanikaev, Nature Photonics **14**, 89 (2020).
- [63] H. Yoshimi, T. Yamaguchi, Y. Ota, Y. Arakawa and S. Iwamoto, Optics Letters **45**, 2648 (2020).
- [64] M. Kim, Z. Jacob and J. Rho, Light: Science and Applications **9**, 130 (2020).
- [65] S. Iwamoto, Y. Ota and Y. Arakawa, Optical Materials Express **11**, 319 (2021).
- [66] X. Zhu, H. Wang, S. K. Gupta, H. Zhang, B. Xie, M. Lu, and Y. Chen, Phys. Rev. Research **2**, 013280 (2020).
- [67] Y. Song, W. Liu, L. Zheng, Y. Zhang, B. Wang and P. Lu, Phys. Rev. Applied **14**, 064076 (2020).
- [68] A. Szameit, D. Blöer, J. Burghoff, T. Schreiber, T. Pertsch, S. Nolte, A. Tünnermann and F. Lederer, Optics Express **13**, 10552 (2005).
- [69] D. N. Christodoulides, F. Lederer and Y. Silberberg, Nature **424**, 817 (2003).
- [70] N. Hatano and D. R. Nelson, Phys. Rev. Lett. **77**, 570 (1996): Phys. Rev. B **56**, 8651 (1997): Phys. Rev. B **58**, 8384 (1998).
- [71] M. Ezawa, Phys. Rev. B **100**, 165419 (2019).
- [72] K. Kawabata, K. Shiozaki, M. Ueda, and M. Sato, Phys. Rev. X **9**, 041015 (2019).
- [73] B. A. Bhargava, I. C. Fulga, J. van den Brink and A. G. Moghaddam, Phys. Rev. B **104**, L241402 (2021).
- [74] F. Schindler and A. Prem, Phys. Rev. B **104**, L161106 (2021)
- [75] C. Yuce, Phys. Lett. A **408**, 127484 (2021)